2-3-2021

Sulfolane-Induced Supercharging of Electrosprayed Salt Clusters: An Experimental/Computational Perspective.

Leanne M Martin

Lars Konermann

Sulfolane-Induced Supercharging of Electrosprayed Salt Clusters: An Experimental/Computational Perspective

Leanne M. Martin and Lars Konermann*

Department of Chemistry, The University of Western Ontario, London, Ontario, N6A 5B7, Canada.

* corresponding author: konerman@uwo.ca

Funding was provided by the Natural Sciences and Engineering Research Council of Canada (RGPIN-2018-04243).

ABSTRACT: It is well known that supercharging agents (SCAs) such as sulfolane enhance the electrospray ionization (ESI) charge states of proteins, although the mechanistic origins of this effect remain contentious. Only very few studies have explored SCA effects on analytes other than proteins or peptides. This work examines how sulfolane affects electrosprayed NaI salt clusters. Such alkali metal halide clusters have played a key role for earlier ESI mechanistic studies, making them interesting targets for supercharging investigations. ESI of aqueous NaI solutions predominantly generated singly charged $[Na_n I_{(n-1)}]^+$ clusters. Addition of sulfolane resulted in abundant doubly charged $[Na_n I_{(n-2)} Sulfolane_s]^{2+}$ species. These experimental data for the first time demonstrate that electrosprayed salt clusters can undergo supercharging. Molecular dynamics (MD) simulations of aqueous ESI nanodroplets containing Na^+/I^- with and without sulfolane were conducted to obtain atomistic insights into the supercharging mechanism. The simulations produced $[Na_n I_i]^{z+}$ and $[Na_n I_i Sulfolane_s]^{z+}$ clusters similar to those observed experimentally. The MD trajectories demonstrated that these clusters were released into the gas phase upon droplet evaporation to dryness, in line with the charged residue model. Sulfolane was found to evaporate much more slowly than water. This slow evaporation, in conjunction with the large dipole moment of sulfolane, resulted in electrostatic stabilization of the shrinking ESI droplets and the final clusters. Hence, charge-dipole stabilization causes the sulfolane-containing droplets and clusters to retain more charge, thereby providing the mechanistic foundation of salt cluster supercharging.

Introduction

Electrospray ionization (ESI) mass spectrometry (MS) is an essential tool for studying a wide range of analytes, from atomic ions to large biomolecular complexes [1-3]. The ESI source produces charged droplets. Solvent evaporation and fission events reduce the droplet size to the nanometer radii, followed by analyte ion release into the gas phase [4]. Many facets of these analyte release steps remain unclear [5-16], although consensus has started to emerge regarding several core issues [3,4,17]. Small pre-charged analytes undergo ejection from the droplet surface, as described by the ion evaporation model (IEM) [6,8]. Large globular analytes such as folded proteins during native ESI tend to follow the charged residue model (CRM) which involves droplet evaporation to dryness [2,3,9]. Less commonly, folded proteins show IEM behavior [12,18]. Unfolded proteins likely follow the chain ejection model (CEM), which involves the gradual expulsion of stretched-out chains from the droplet surface [17]. CEM behavior has also been proposed for disordered synthetic polymers [19,20].

A key property of electrosprayed biomolecular ions is their charge state z. High charge states are often associated with beneficial features such as enhanced ion transmission [21] and fragmentation [22,23], high reactivity [24-26], and resolution improvements on Fourier-transform instruments including Orbitraps [27,28]. Not surprisingly, strategies to manipulate analyte charge states have attracted considerable interest, particularly for proteins and peptides [25,29-35].

One way to boost protein ESI charge states is to use denaturing conditions that cause unfolding in bulk solution [17,36,37]. A complementary approach that has attracted a lot of attention in recent years involves organic supercharging agents (SCAs, such as sulfolane, *m*-nitrobenzyl alcohol, and alkyl carbonates) [32,38-42]. SCAs are added at concentrations that are low enough to leave bulk solution protein structures unchanged [43]. The low vapor pressure of SCAs causes them to evaporate more slowly than water, causing the shrinking ESI droplets to undergo SCA enrichment

[16,43-45]. SCAs have large dipole moments, e.g., 4.7 D for sulfolane vs. 1.85 D for water [45-49]. In addition to at least one highly polar functional group, SCAs contain a nonpolar moiety [17,44,45]. Their surface tension is between methanol and water [45], and their Brønsted basicity is low [48].

For clarity, we emphasize that SCAs are neutral molecules. Thus, supercharging is *not* caused by the trivial adduction of analytes with charged moieties. Instead, SCAs exert their effects in more subtle ways by interfering with the ESI process. The exact mechanisms by which SCAs enhance charge states remain contentious. SCAs boost protein charge under both native [44,50] and denaturing ESI conditions [25,45,49]. The underlying mechanisms are likely different in these two scenarios [17]. Initial mechanistic ideas focused on surface tension [11], but subsequent studies concluded that this factor is not a major contributor [44,51]. Alternatively, it was suggested that native supercharging might be caused by protein unfolding in the droplet [43], a proposal that appears to be at odds with the observation of supercharged proteins that retain compact conformations and native binding interactions [38,44,52-54]. Molecular dynamics (MD) simulations indicated that native supercharging is caused by SCA accumulation at the droplet surface. This SCA surface layer suppresses the ejection of small charge carriers from the droplet (such as H^+_{aq} and Na^+_{aq}), such that CRM-produced macroions retain more charge as the droplets dry out [17]. Denaturing ESI supercharging experiments found that protein ions are formed via the CEM [40], and that supercharging involves direct protein-SCA contacts [49]. Both of these features are consistent with MD data that revealed the electrostatic stabilization of protonated side chains by SCA adducts [17].

The aforementioned supercharging investigations focused almost exclusively on proteins or peptides, while supercharging studies on other analytes are scarce [55]. The current work aims to contribute to a better understanding of supercharging by examining a completely different type of analyte, i.e., alkali metal halide clusters. Our interest in these clusters reflects the fact that these

species have played a central role for earlier mechanistic studies of the ESI process [10,13,56-62]. As a typical example, $[Na_n\ Cl_m]^{(n-m)+}$ clusters are formed when electrospraying aqueous NaCl solutions. Practitioners are familiar with such clusters because of their use as mass calibrants [63,64], as well as a source of chemical noise for improperly desalted samples [65]. The presence of alkali metal halide clusters in ESI mass spectra is non-trivial, because these salts are highly soluble and exist as completely dissociated (single) ions in bulk aqueous solution, implying that the clusters are generated during ESI. Previous studies have explained this phenomenon by suggesting that the clusters are CRM products that form when cations/anions associate with one another while the final nanodroplets evaporate to dryness [10,56,66,67].

To the best of our knowledge, it is not known how ESI-generated salt clusters respond to the presence of SCAs. Several questions remain unanswered. Will the charge states of salt clusters increase? What are the mechanisms by which SCAs affect the ESI process for salt solutions? Is supercharging a phenomenon that is limited to biological polymers?

The current work focuses on ESI-generated NaI clusters because naturally occurring ^{23}Na and ^{127}I are isotopically pure [64], thereby producing relatively simple mass distributions (other salts tend to yield highly convoluted isotope patterns that are more difficult to interpret). The supercharging experiments discussed here employed sulfolane, $(CH_2)_4SO_2$, a prototypical SCA that is widely used for proteins [17,44,45]. Our investigations employed positive ion mode, which is most commonly used for most ESI applications. The results obtained reveal that ESI-generated NaI clusters show elevated charge states in the presence of sulfolane. MD simulations suggest that the formation of these supercharged salt clusters results from dipole-mediated electrostatic stabilization.

Materials and Methods

ESI-MS and IMS. ESI-MS experiments were performed on a SYNAPT G2 quadrupole time-of-flight mass spectrometer (Waters, Milford, MA). Aqueous solutions containing 10 mM NaI were infused into the ESI source at 5 μL min^{-1}. For supercharging, the solutions were supplemented with 5% (v/v) sulfolane. Unless noted otherwise, gentle source conditions were used to prevent cluster dissociation. For this purpose, the ESI source was operated at +1.6 kV, the source and desolvation temperatures were 30 and 40 °C, respectively, and the cone was set to 5 V. Travelling wave ion mobility spectrometry (IMS) was used to separate singly and doubly charged clusters that shared the same monoisotopic *m/z*. For IMS the Triwave was enabled (trap DC entrance 0 V, trap DC bias 15 V, trap DC -2 V, trap DC exit 1 V, IMS DC entrance 6.7 V, He cell DC 10 V, He exit -5 V, IMS bias 3 V, IMS DC exit 0 V, transfer DC entrance 1 V, transfer DC exit 1 V, trap wave velocity 100 m s^{-1}, trap wave height 1 V, IMS wave velocity 450 m s^{-1}, IMS wave height 8 V, transfer wave velocity 247 m s^{-1}, and transfer wave height 4 V). Isotope distributions were modeled using the Scientific Instrument Services isotopic abundance calculator (sisweb.com/mstools/isotope.htm).

MD Simulations. MD simulations of ESI droplets were conducted by following established methods [17] using Gromacs 2019 [68] with the CHARMM36 forcefield [69] and TIP4P/2005 water [70]. Droplets with 3 nm radius were assembled (~2600 water or ~2300 water / 200 sulfolane molecules) and charged by inserting Na^+ and I^- ions in random positions. Different numbers of Na^+ and I^- were tested, but the initial droplet charge was always 18+, which corresponds to the Rayleigh limit for droplets in this size regime [4]. After energy minimization and equilibration, MD runs were performed for 200 ns at 370 K, followed by 100 ns at 450 K to speed up solvent evaporation, for a total simulation time of 300 ns. ESI charge states were determined by tallying the number of Na^+ and I^- within the final clusters. All runs were repeated five times for each type of simulation, with

different initial ion and sulfolane positions, and different initial atom velocities. Lennard-Jones parameters for Na^+ were used as predefined in CHARMM36 [69], and parameters for I^- were taken from the literature ($\varepsilon = 0.656496$ kJ mol^{-1}, $\sigma = 0.519226$ nm) [71]. The resulting MD bond length of an isolated Na-I unit (2.9 Å) at 0 K was close to that obtained from density functional theory (2.73 Å) [72], supporting the appropriateness of these Lennard-Jones parameters.

Results and Discussion

ESI-Generated NaI Clusters from Aqueous Solution. ESI of aqueous NaI solutions (without sulfolane) mainly generated singly charged $[Na_n I_{(n-1)}]^+$ clusters. Close inspection of the higher mass range (beyond *m/z* 1400) also revealed doubly charged $[Na_n I_{(n-2)}]^{2+}$ clusters in low abundance (Figure 1A). These observations are consistent with previous work [63,64]. Our data confirm that bare 2+ clusters can exist only above a certain size [58,73]. The smallest 2+ cluster produced from aqueous solution is $[Na_{17} I_{15}]^{2+}$ (arrow in Figure 1A). Smaller 2+ clusters are unstable because of their high charge density [58,73].

ESI-Generated NaI Clusters from Water/Sulfolane Solution. Spiking of NaI solutions with 5% sulfolane resulted in ESI mass spectra with abundant $[Na_n I_i \text{ Sulfolane}_s]^{(n-i)+}$ clusters, where n = number of Na^+, i = number of I^-, and s = number of sulfolane (Figure 1B, C). These spectra were dominated by 2+ clusters covering the range between *m/z* 900 and 2200. There were also contributions from 3+ species at $m/z > 1600$, and some singly charged clusters at $m/z < 1000$. These experiments demonstrate that sulfolane significantly boosts the charge states of NaI clusters, from mostly 1+ in water (Figure 1A) to mostly 2+ in the presence of the SCA (Figure 1B, C). In other

words, sulfolane causes supercharging of ESI-generated NaI clusters. It appears that this is the first observation of SCA-induced charge enhancement for ESI-generated salt clusters.

In addition to boosting charge, sulfolane also increased the NaI cluster size. For the 1+ clusters of Figure 1A the number of I^- extends to $i \approx 14$, whereas the 2+ clusters in Figure 1B, C go up to $i \approx 23$. These size differences may reflect the lower NaI solubility in sulfolane compared to water [74]. Specifically, sulfolane enrichment in shrinking ESI droplets [16,43-45] could promote the precipitation of Na^+ and I^- into larger NaI clusters. This scenario raises an interesting question: Is NaI supercharging a trivial cluster size effect, keeping in mind that larger clusters can support more charge [58,73]? A closer look reveals that this explanation alone *cannot* account for the experimentally observed behavior. This becomes clear when comparing clusters of similar size generated with and without sulfolane. For example, all clusters with $i = 9$ generated from water have a 1+ charge (Figure 1A). In contrast, all $i = 9$ clusters from water/sulfolane carry a 2+ charge (Figure C). Analogous considerations apply for many other clusters from $i = 6$ to $i = 14$ in Figure 1. In all these cases sulfolane doubles the charge for any given value of i. In addition, sulfolane dramatically lowers the size of the smallest observable 2+ cluster, from $i = 15$ to $i = 6$ (arrows in Figure 1). We conclude that cluster size may contribute to the charge enhancement seen in Figure 1; however, this "trivial" factor is not the root cause of sulfolane-induced NaI supercharging.

The retention of sulfolane in supercharged NaI clusters ($s = 5$-7 for 2+, $s = 8$ for 3+) indicates that the charge enhancement mechanism involves direct analyte/sulfolane interactions. This assertion is reminiscent of proposals made in the context of protein supercharging [17,49]. However, in contrast to the $[Na_n I_i \text{Sulfolane}_s]^{(n-i)+}$ clusters seen here, supercharged proteins tend to lose SCA adducts during ion sampling [17,32,38-42,49].

Collisional Activation of Supercharged Clusters. The spectra of Figure 1 were acquired under gentle ion sampling conditions, with the cone set to 5 V Raising the cone voltage from 5 V to 100 V caused collisional heating of the $[Na_n\ I_i\ Sulfolane_s]^{(n-i)+}$clusters. These conditions caused neutral loss of sulfolane, accompanied by a decrease in cluster size to roughly half their initial values (in terms of *n* and *i*). The products formed after this activation step were singly charged $[Na_n\ I_{(n-1)}]^+$ ions (Figure 2). The disappearance of highly charged (2+/3+) clusters is in line with the fact that higher charge states are generally more prone to CID [58]. It is nonetheless interesting that the singly charged NaI clusters did not retain any sulfolane. The data of Figure 2 are thus consistent with the idea that the viability of NaI clusters with $z > 1$ depends on sulfolane adduction, as indicated by the data in the preceding section. We will examine the significance of sulfolane binding to the supercharged clusters in more detail below.

Ion Mobility Spectrometry and Isotope Distributions. IMS was used to examine the ESI-generated clusters of Figure 1 in more detail. Singly charged clusters produced in the absence of sulfolane had unimodal IMS profiles, illustrated for $[Na_6\ I_5]^+$ in Figure 3A. The ~100% isotopic purity of Na^+ and I^- translated into mass spectra with single isolated peaks (Figure 3B). Unimodal IMS profiles were also observed for many of the clusters generated in the presence of sulfolane, exemplified for $[Na_{11}\ I_9\ Sulfolane_6]^{2+}$ in Figure 3C. The $^{12/13}C$ heterogeneity of sulfolane caused isotope distributions, such that the cluster charge could be determined directly from the spectra. The 2+ species in Figure 3D had a peak spacing of $\Delta m/z = 0.5$. Interestingly, there were also instances of sulfolane-containing clusters with bimodal IMS profiles, exemplified in Figure 3E for species with a monoisotopic *m/z* of 982.6. Spectra extracted from the two IMS features revealed overlapping 2+ and 1+ contributions, i.e., $[Na_{10}\ I_8\ Sulfolane_6]^{2+}$ with $\Delta m/z = 0.5$ (Figure 3F) and $[Na_5\ I_4\ Sulfolane_3]^+$ with $\Delta m/z = 1$ (Figure 3G).

Overlap of 2+ and 1+ clusters is possible only for $[Na_n I_i Sulfolane_s]^{2+}$ clusters with even-numbered *n*, *i*, and *s*. Such conditions allow for the existence of a 1+ cluster with *n*/2, *i*/2, *s*/2 at the same monoisotopic *m/z*. In contrast, for 2+ species with one or more uneven *n*, *i*, *s* the existence of an overlapping 1+ cluster is mathematically not possible. This latter scenario applies to more than half of the annotated peaks in Figure 1C. In summary, the IMS data and isotope distributions discussed here reaffirm that sulfolane promotes the formation of doubly charged clusters, while spectra acquired without sulfolane are dominated by singly charged clusters.

Molecular Dynamics Simulations. Previous studies have demonstrated that MD simulations of nanodroplets can reveal the mechanisms of gas phase ion formation under various ESI conditions [17,75-83]. Here we used this approach to elucidate how sulfolane causes supercharging of NaI clusters. Our simulations examined droplets with an initial radius of 3 nm, matching the size regime of late nanodroplets in the ESI plume [4]. The initial 18+ droplet charge corresponds to the Rayleigh limit, in line with experiments [4,9,84].

We will first discuss MD data for droplets that initially contained 38 Na^+ and 20 I^-. Typical trajectory snapshots are illustrated in Figure 4. The events observed with and without sulfolane shared a number of similarities. All droplets rapidly shrank due to solvent evaporation, culminating in the formation of clusters (top to bottom in Figure 4). The formation of these clusters in the MD runs is consistent with the observation of cluster ions in the experiments of Figure 1. $[Na_n I_i]^{(n-i)+}$ and $[Na_n I_i Sulfolane_s]^{(n-i)+}$ clusters assembled during the final stages of droplet evaporation, which implies that they form via the CRM. This finding echoes earlier studies which also concluded that ESI-generated clusters are CRM products [10,56,66,67]. Early during the runs the droplets underwent frequent ejection of Na^+ ions that were solvated by a few water or water/sulfolane molecules. These ion ejection events are consistent with the IEM [4,6,8,17]. Most of these IEM

events involved a single Na^+, but there were also a few instances where two Na^+ left the droplet together (Figure 4B, t = 0.25 ns). I^- loss was uncommon, reflecting the electrostatic attraction between these anions and the positively charged droplets. On rare occasion, I^- were ejected as solvated Na_2I^+.

Despite these commonalities, Figure 4 also reveals significant differences for MD runs conducted with and without sulfolane. Water evaporated rapidly, while sulfolane departed much more slowly as expected from its low vapor pressure [16,43-45]. At the end of the 300 ns simulation window the water droplet in Figure 4A had transformed into a desolvated $[Na_{22}\ I_{20}]^{2+}$ cluster. In contrast, the water/sulfolane droplet of Figure 4B had evaporated into a $[Na_{23}\ I_{20}\ Sulfolane_{23}]^{3+}$ cluster, with a salt core and a shell of residual sulfolane molecules.

Figure 5 takes a closer look at the temporal evolution of droplets that initially contained 38 Na^+ and 20 I^-. For water droplets, Na^+ were ejected while H_2O evaporated (Figure 5A,B), and the $[Na_n\ I_i]^{(n-i)+}$ clusters attained their final composition as the final H_2O molecules departed. Water/sulfolane droplets showed rapid water loss early during the run, but there was relatively little sulfolane evaporation until the temperature was raised to 450 K at t = 200 ns (Figure 5C,D). IEM ejection of sulfolane-bound Na^+ continued after all the water had left (Figure 5D).

Charge Progression in Water vs. Water/Sulfolane Droplets. The most salient feature in the MD data of Figure 5 is that the shrinking droplets retained a higher charge in the presence of sulfolane at any given time point. For example, at t = 100 ns water/sulfolane runs exhibited a charge of (7.6 ± 0.5)+, while for the water runs the charge had dropped to (2 ± 0)+ at this point. Very similar effects were seen for simulations with other initial Na^+/ I^- compositions (Figure S1).

The strikingly different charge loss kinetics for water vs. water/sulfolane are further highlighted in Figure 6. These differences were most pronounced between 100 ns and 200 ns, where

the water/sulfolane systems retained two to three times more charge than the water runs (Figure 6A, B). In this range, the water droplets had already transformed into clusters that were almost solvent-free, while more than 100 sulfolane molecules were retained for water/sulfolane runs. Subsequent sulfolane evaporation promoted charge loss via Na^+ IEM events, thereby gradually diminishing the charge of the sulfolane-surrounded salt clusters. At the end of the MD runs (t = 300 ns) between 12 and 26 sulfolane molecules remained. Most of the final sulfolane-containing clusters carried one additional charge compared to clusters generated from water droplets (Figure 6C). Only for runs with the lowest ion concentration (26 Na^+/8 I^-) both droplet types shared the same final charge state.

Comparing Simulated and Experimental Results. Our MD data reproduce two key trends seen in the experiments of Figure 1. (i) Simulated sulfolane/water droplets generated NaI clusters that retained some sulfolane, while water droplets yielded completely desolvated NaI assemblies. (ii) Clusters produced from sulfolane-containing droplets were more highly charged than those formed from pure water droplets, i.e., sulfolane caused supercharging. It is gratifying that these experimentally observed trends are reproduced by the MD runs, providing the opportunity to examine the mechanism of sulfolane-induced supercharging (see discussion below).

An honest appraisal of our results, however, must acknowledge that the agreement between MD and experimental data is qualitative, rather than quantitative. Across the board, the MD-generated final charge states were somewhat higher than those observed experimentally. For example, MD runs with 38 Na^+/20 I^- in water produced 2+ clusters (Figure 6C) while the corresponding experimental data were dominated by 1+ ions with low intensity 2+ contributions (Figure 1A). Water/sulfolane simulations yielded clusters with a charge state of (2.8 ± 0.4)+, whereas the corresponding experiments showed abundant 2+ ions and low intensity 3+ contributions (Figure 1B, C). It is possible that these deviations arise from the large polarizability of I^- [85] which

is difficult to model when using classical force fields of the type employed here and for previous ESI simulations [17,75-83].

Mechanism of NaI Cluster Supercharging. Why does the presence of sulfolane generate NaI clusters with a higher net charge? Sulfolane has a very large dipole moment of 4.7 D [45-49] that results from the asymmetric distribution of atomic partial charges in the $(CH_2)_4SO_2$ ring. The two oxygens possess the highest electron density and represent the negative end of the sulfolane dipole (Figure 7A). In the $[Na_n\ I_i\ Sulfolane_s]^{(n-i)+}$ clusters the sulfolane molecules solvate the positively charged cluster core by pointing their negative ends toward Na^+ ions. Figure 7B zooms into these charge-dipole contacts for a typical MD-generated 3+ cluster at t = 300 ns. Inspection of Figure 4B shows that this trend also holds for shrinking droplets throughout the ESI process; in all cases the sulfolane molecules tend to point their oxygens toward the positively charged droplet interior. Figure 7C illustrates this charge solvation as a simplified cartoon.

Charge-dipole solvation is a common occurrence in many different systems. For example, Na^+ in bulk water is tightly surrounded by a solvation shell where H_2O dipoles point their oxygens toward the central cation [86]. Similarly, inter- and intramolecular charge solvation plays a major role for the behavior of gaseous proteins [87-89]. In all those examples, charge-dipole contacts exert a stabilizing effect that lowers the overall energy of the system.

We scrutinized the magnitude of charge-dipole solvation in MD-generated Na^+/I^-/sulfolane droplets and clusters by calculating their total electrostatic energy V_{tot} according to

$$V_{tot} = \sum_{i>j} \frac{1}{4\pi\varepsilon_0} \frac{q_i q_j}{r_{ij}} \qquad (1)$$

where q_i and q_j refer to the charges of atoms and ions, and r_{ij} are the corresponding distances. The summation included all atoms and ions, excluding intramolecular contacts within the same sulfolane

molecule. The reference point for these calculations is $V_{tot} = 0$, which represents the situation where all Na^+, I^-, and sulfolanes are infinitely far apart.

The results of these electrostatic calculations are compiled in Figure 7D, focusing on MD results for droplets that initially contained 38 Na^+ and 20 I^-. The calculations were performed under two conditions, (i) for intact systems with sulfolane present (solid bars), and (ii) after removal of sulfolane (open bars). Figure 7D shows that sulfolane causes a dramatic electrostatic stabilization of late ESI droplets. For t = 100 ns and 200 ns sulfolane rendered the Na^+/I^-/sulfolane droplets twice as stable, by lowering their V_{tot} from roughly -10,000 kJ mol^{-1} to -20,000 kJ mol^{-1}. For the final t = 300 ns clusters this stabilizing effect was somewhat diminished because they contained less sulfolane, but V_{tot} was still lowered by ~17%.

Overall, the V_{tot} calculations of Figure 7D reveal that sulfolane causes supercharging by stabilizing late ESI nanodroplets while they gradually transition into the final $[Na_n I_i \text{Sulfolane}_s]^{(n-i)+}$ clusters. Electrostatic stabilization lowers the propensity of the shrinking droplets to undergo Na^+ IEM ejection, thereby imparting a higher net charge to the final CRM-generated cluster.

Conclusions

This work for the first time demonstrates that a typical "protein SCA" such as sulfolane [17,44,45] is also capable of inducing supercharging for alkali metal halide clusters which represent a completely different type of ESI-MS analyte. The physicochemical characteristics that allow sulfolane to cause NaI cluster supercharging are its low vapor pressure and large dipole moment. The former ensures that residual sulfolane remains tightly associated with the NaI cluster until the end of the ESI process. The latter causes electrostatic stabilization via charge-dipole solvation that facilitates the survival of highly charged clusters. In comparison, water cannot stabilize NaI clusters

to the same extent; although H_2O provides excellent charge solvation [86] it departs early during the ESI process because it is more volatile than sulfolane.

The NaI cluster supercharging mechanism uncovered here involves several elements that have previously been discussed in the context of protein supercharging models. Specifically, the capability of sulfolane-containing droplets to retain a large amount of charge is analogous to the "charge trapping mechanism" that has been proposed for native ESI supercharging of proteins [17]. In addition, the central role of dipole-induced charge stabilization via direct SCA-analyte contacts has been shown to be essential for protein supercharging under denaturing conditions [17,49].

Overall, this work is part of a growing number of studies from multiple laboratories that use MD strategies for examining mechanistic aspects of ESI and other MS-related processes. It is hoped that research in this exciting area will continue to promote a synergistic relationship between experimental and computational approaches.

References

1. Fenn, J.B.: Electrospray Wings for Molecular Elephants (Nobel Lecture). *Angew. Chem. Int. Ed.* **42,** 3871-3894 (2003)

2. Leney, A.C., Heck, A.J.R.: Native Mass Spectrometry: What is in the Name? *J. Am. Soc. Mass Spectrom.* **28,** 5-13 (2017)

3. Mehmood, S., Allison, T.M., Robinson, C.V.: Mass Spectrometry of Protein Complexes: From Origins to Applications. *Annu. Rev. Phys. Chem.* **66,** 453-474 (2015)

4. Kebarle, P., Verkerk, U.H.: Electrospray: From Ions in Solutions to Ions in the Gas Phase, What We Know Now. *Mass Spectrom. Rev.* **28,** 898-917 (2009)

5. Dole, M., Mack, L.L., Hines, R.L., Mobley, R.C., Ferguson, L.D., Alice, M.B.: Molecular beams of macroions. *J. Chem. Phys.* **49,** 2240-2249 (1968)

6. Iribarne, J.V., Thomson, B.A.: On the evaporation of small ions from charged droplets. *J. Chem. Phys.* **64,** 2287-2294 (1976)

7. Siu, K.W.M., Guevremont, R., Le Blanc, J.C.Y., O'Brien, R.T., Berman, S.S.: Is Droplet Evaporation Crucial in the Mechanism of Electrospray Mass Spectrometry? *Org. Mass Spectrom.* **28,** 579-584 (1993)

8. Loscertales, I.G., de la Mora, J.F.: Experiments on the kinetics of field evaporation of small ions from droplets. *J. Chem. Phys.* **103,** 5041-5060 (1995)

9. de la Mora, J.F.: Electrospray Ionization of large multiply charged species proceeds via Dole's charged residue mechanism. *Anal. Chim. Acta* **406,** 93-104 (2000)

10. Wang, G., Cole, R.B.: Charged residue versus ion evaporation for formation of alkali metal halide clusters ions in ESI. *Anal. Chim. Acta* **406,** 53-65 (2000)

11. Iavarone, A.T., Williams, E.R.: Mechanism of Charging and Supercharging Molecules in Electrospray Ionization. *J. Am. Chem. Soc.* **125,** 2319-2327 (2003)

12. Nguyen, S., Fenn, J.B.: Gas-phase ions of solute species from charged droplets of solutions. *Proc. Natl. Acad. Sci. U.S.A.* **104,** 1111-1117 (2007)

13. Spencer, E.A.C., Ly, T., Julian, R.K.: Formation of the serine octamer: Ion evaporation or charge residue? *Int. J. Mass Spectrom.* **270,** 166-172 (2008)

14. Hogan, C.J., Carroll, J.A., Rohrs, H.W., Biswas, P., Gross, M.L.: Combined Charged Residue-Field Emission Model of Macromolecular Electrospray Ionization. *Anal. Chem.* **81,** 369-377 (2009)

15. Marchese, R., Grandori, R., Carloni, R., Raugei, S.: A Computational Model for Protein Ionization by Electrospray Based on Gas-Phase Basicity. *J. Am. Soc. Mass Spectrom.* **23,** 1903-1910 (2012)

16. Ogorzalek Loo, R.R., Lakshmanan, R., Loo, J.A.: What Protein Charging (and Supercharging) Reveal about the Mechanism of Electrospray Ionization. *J. Am. Soc. Mass Spectrom.* **25,** 1675-1693 (2014)

17. Konermann, L., Metwally, H., Duez, Q., Peters, I.: Charging and Supercharging of Proteins for Mass Spectrometry: Recent Insights into the Mechanisms of Electrospray Ionization. *Analyst* **144,** 6157-6171 (2019)

18. Aliyari, E., Konermann, L.: Formation of Gaseous Proteins via the Ion Evaporation Model (IEM) in Electrospray Mass Spectrometry. *Anal. Chem.* **92,** 10807-10814 (2020)

19. Consta, S., Chung, J.K.: Charge-Induced Conformational Changes of PEG-(Na+)n in Vacuum and Aqueous Nanodroplets. *J. Phys. Chem. B* **115,** 10447-10455 (2011)

20. Duez, Q., Metwally, H., Hoyas, S., Lemaur, V., Cornil, J., De Winter, J., Konermann, L., Gerbaux, P.: Effects of electrospray mechanisms and structural relaxation on polylactide ion conformations in the gas phase: insights from ion mobility spectrometry and molecular dynamics simulations. *Phys. Chem. Chem. Phys.* **22,** 4193-4204 (2020)

21. Covey, T.R., Thomson, B.A., Schneider, B.B.: Atmospheric Pressure Ion Sources. *Mass Spectrom. Rev.* **28,** 870-897 (2009)

22. Yin, S., Loo, J.A.: Top-down mass spectrometry of supercharged native protein–ligand complexes. *Int. J. Mass Spectrom.* **300,** 118-122 (2011)

23. Compton, P.D., Zamdborg, L., Thomas, P.M., Kelleher, N.L.: On the Scalability and Requirements of Whole Protein Mass Spectrometry. *Anal. Chem.* **83,** 6868-6874 (2011)

24. McLuckey, S.A., Van Berkel, G.J., Glish, G.L.: Reactions of Dimethylamine with Multiply Charged Ions of Cytochrome c. *J. Am. Chem. Soc.* **112,** 5668-5670 (1990)

25. Ke, M.F., Zhang, H., Ding, J.H., Xiong, X.C., Li, F.L., Chingin, K., Kou, W., Liu, A.Y., Zhu, T.G., Fang, X., Chen, H.W.: Generating Supercharged Protein Ions for Breath Analysis by Extractive Electrospray Ionization Mass Spectrometry. *Anal. Chem.* **91,** 3215-3220 (2019)

26. Zenaidee, M.A., Leeming, M.G., Zhang, F.T., Funston, T.T., Donald, W.A.: Highly Charged Protein Ions: The Strongest Organic Acids to Date. *Angew. Chem.-Int. Edit.* **56,** 8522-8526 (2017)

27. Marshall, A.G., Hendrickson, C.L., Jackson, G.S.: Fourier Transform Ion Cyclotron Resonance Mass Spectrometry: A Primer. *Mass Spectrom. Rev.* **17,** 1-35 (1998)

28. Zubarev, A.R., Makarov, A.: Orbitrap Mass Spectrometry. *Anal. Chem.* **85,** 5288-5296 (2013)

29. Kharlamova, A., Prentice, B.M., Huang, T.-Y., McLuckey, S.A.: Electrospray Droplet Exposure to Gaseous Acids for the Manipulation of Protein Charge State Distributions. *Anal. Chem.* **82,** 7422-7429 (2010)

30. Lin, C.W., Haeuptle, M.A., Aebi, M.: Supercharging Reagent for Enhanced Liquid Chromatographic Separation and Charging of Sialylated and High-Molecular-Weight Glycopeptides for NanoHPLC-ESI-MS/MS Analysis. *Anal. Chem.* **88,** 8484-8494 (2016)

31. Thinius, M., Polaczek, C., Langner, M., Bräkling, S., Haack, A., Kersten, H., Benter, T.: Charge Retention/Charge Depletion in ESI-MS: Experimental Evidence. *J. Am. Soc. Mass Spectrom.* **31,** 773-784 (2020)

32. Keener, J.E., Zambrano, D.E., Zhang, G.Z., Zak, C.K., Reid, D.J., Deodhar, B.S., Pemberton, J.E., Prell, J.S., Marty, M.T.: Chemical Additives Enable Native Mass Spectrometry Measurement of Membrane Protein Oligomeric State within Intact Nanodiscs. *J. Am. Chem. Soc.* **141,** 1054-1061 (2019)

33. Gong, X.Y., Li, C., Zhai, R., Xie, J., Jiang, Y., Fang, X.: Supercharging of Proteins by Salts during Polarity Reversed Nano-Electrospray Ionization. *Anal. Chem.* **91,** 1826-1837 (2019)

34. Abzalimov, R.R., Kaltashov, I.A.: Electrospray Ionization Mass Spectrometry of Highly Heterogeneous Protein Systems: Protein Ion Charge State Assignment via Incomplete Charge Reduction. *Anal. Chem.* **82,** 7523–7526 (2010)

35. Wang, G., Cole, R.B.: Disparity Between Solution-phase Equilibria and Charge State Distributions in Positive-ion Electrospray Mass Spectrometry. *Org. Mass Spectrom.* **29,** 419-427 (1994)

36. Chowdhury, S.K., Katta, V., Chait, B.T.: Probing Conformational Changes in Proteins by Mass Spectrometry. *J. Am. Chem. Soc.* **112,** 9012-9013 (1990)

37. Dobo, A., Kaltashov, I.A.: Detection of Multiple Protein Conformational Ensembles in Solution via Deconvolution of Charge-State Distributions in ESI MS. *Anal. Chem.* **73,** 4763-4773 (2001)

38. Lomeli, S.H., Yin, S., Loo, R.R.O., Loo, J.A.: Increasing Charge While Preserving Noncovalent Protein Complexes for ESI-MS. *J. Am. Soc. Mass Spectrom.* **20,** 593-596 (2009)

39. Iavarone, A.T., Jurchen, J.C., Williams, E.R.: Supercharged Protein and Peptide Ions Formed by Electrospray Ionization. *Anal. Chem.* **73,** 1455-1460 (2001)

40. Donor, M.T., Ewing, S.A., Zenaidee, M.A., Donald, W.A., Prell, J.S.: Extended Protein Ions Are Formed by the Chain Ejection Model in Chemical Supercharging Electrospray Ionization. *Anal. Chem.* **89,** 5107-5114 (2017)

41. Li, X., Li, Z., Xie, B., Sharp, J.S.: Supercharging by m-NBA Improves ETD-Based Quantification of Hydroxyl Radical Protein Footprinting. *J. Am. Soc. Mass Spectrom.* **26,** 1424-1427 (2015)

42. Meyer, J.G., Komives, E.A.: Charge State Coalescence During Electrospray Ionization Improves Peptide Identification by Tandem Mass Spectrometry. *J. Am. Soc. Mass Spectrom.* **23,** 1390-1399 (2012)

43. Sterling, H.J., Daly, M.P., Feld, G.K., Thoren, K.L., Kintzer, A.F., Krantz, B.A., Williams, E.R.: Effects of Supercharging Reagents on Noncovalent Complex Structure in Electrospray Ionization from Aqueous Solutions. *J. Am. Soc. Mass Spectrom.* **21,** 1762-1774 (2010)

44. Lomeli, S.H., Peng, I.X., Yin, S., Ogorzalek Loo, R.R., Loo, J.A.: New Reagents for Increasing ESI Multiple Charging of Proteins and Protein Complexes. *J. Am. Soc. Mass Spectrom.* **21,** 127-131 (2010)

45. Teo, C.A., Donald, W.A.: Solution Additives for Supercharging Proteins beyond the Theoretical Maximum Proton-Transfer Limit in Electrospray Ionization Mass Spectrometry. *Anal. Chem.* **86,** 4455-4462 (2014)

46. Tilstam, U.: Sulfolane: A Versatile Dipolar Aprotic Solvent. *Org. Process Res. Dev.* **16,** 1273-1278 (2012)

47. Liu, H.C., Wang, Y.M., Bowman, J.M.: Transferable ab Initio Dipole Moment for Water: Three Applications to Bulk Water. *J. Phys. Chem. B* **120,** 1735-1742 (2016)

48. Nshanian, M., Lakshmanan, R., Chen, H., Ogorzalek Loo, R.R., Loo, J.A.: Enhancing sensitivity of liquid chromatography–mass spectrometry of peptides and proteins using supercharging agents. *Int. J. Mass Spectrom.* **427,** 157–164 (2018)

49. Douglass, K.A., Venter, A.R.: Investigating the role of adducts in protein supercharging with sulfolane. *J. Am. Soc. Mass Spectrom.* **23,** 489-497 (2012)

50. Hall, Z., Politis, A., Bush, M.F., Smith, L.J., Robinson, C.V.: Charge-State Dependent Compaction and Dissociation of Protein Complexes: Insights from Ion Mobility and Molecular Dynamics. *J. Am. Chem. Soc.* **134,** 3429-3438 (2012)

51. Samalikova, M., Grandori, R.: Protein Charge-State Distributions in Electrospray-Ionization Mass Spectrometry Do Not Appear To Be Limited by the Surface Tension of the Solvent. *J. Am. Chem. Soc.* **125,** 13352-13353 (2003)

52. Hall, Z., Robinson, C.V.: Do Charge State Signatures Guarantee Protein Conformation? *J. Am. Soc. Mass Spectrom.* **23,** 1161-1168 (2012)

53. Hogan, C.J., Ogorzalek Loo, R.R., Loo, J.A., de la Mora, J.F.: Ion mobility-mass spectrometry of phosphorylase B ions generated with supercharging reagents but in charge-reducing buffer. *Phys. Chem. Chem. Phys.* **12,** 13476-13483 (2010)

54. Sterling, H.J., Kintzer, A.F., Feld, G.K., Cassou, C.A., Krantz, B.A., Williams, E.R.: Supercharging Protein Complexes from Aqueous Solution Disrupts their Native Conformations. *J. Am. Soc. Mass Spectrom.* **23,** 191-200 (2012)

55. Xu, N., Chingin, K., Chen, H.W.: Ionic strength of electrospray droplets affects charging of DNA oligonucleotides. *J. Mass Spectrom.* **49,** 103-107 (2014)

56. Juraschek, R., Dulcks, T., Karas, M.: Nanoelectrospray - More than just a Minimized-Flow Electrospray Ionization Source. *J. Am. Soc. Mass Spectrom.* **10,** 300-308 (1999)

57. Hao, C.Y., March, R.E., Croley, T.R., Smith, J.C., Rafferty, S.P.: Electrospray ionization tandem mass spectrometric study of salt cluster ions. Part 1 - Investigations of alkali metal chloride and sodium salt cluster ions. *J. Mass Spectrom.* **36,** 79-96 (2001)

58. Zhang, D.X., Cooks, R.G.: Doubly charged cluster ions (NaCl)(m)(Na)(2) (2+): magic numbers, dissociation, and structure. *Int. J. Mass Spectrom.* **195,** 667-684 (2000)

59. Wakisaka, A.: Nucleation in alkali metal chloride solution observed at the cluster level. *Faraday Discuss.* **136,** 299-308 (2007)

60. Zhang, H., Wei, Z.W., Jiang, J., Cooks, R.G.: Nebulization Prior to Isolation, Ionization, and Dissociation of the Neutral Serine Octamer Allows Its Characterization. *Angew. Chem.-Int. Edit.* **57,** 17141-17145 (2018)

61. Seo, J., Warnke, S., Pagel, K., Bowers, M.T., von Helden, G.: Infrared spectrum and structure of the homochiral serine octamer-dichloride complex. *Nat. Chem.* **9,** 1263-1268 (2017)

62. Zhang, J.C., Bogdanov, B., Parkins, A., McCallum, C.M.: Observation of Magic Number Clusters from Thermal Dissociation Molecular Dynamics Simulations of Lithium Formate Ionic Clusters. *J. Phys. Chem. A* **124,** 3535-3541 (2020)

63. Hop, C.E.C.A.: Generation of high molecular weight cluster ions by electrospray ionization; Implications for mass calibration. *J. Mass Spectrom.* **31,** 1314-1316 (1996)

64. Anacleto, J.F., Pleasance, S., Boyd, R.K.: Calibration of ion spray mass spectra using cluster ions. *Org. Mass Spectrom.* **27,** 660-666 (1992)

65. Xu, N., Lin, Y., Hofstadler, S.A., Matson, D., Call, C.J., Smith, R.D.: A Microfabricated Dialysis Device for Sample Cleanup in Electrospray Ionization Mass Spectrometry. *Anal. Chem.* **70,** 3553-3556 (1998)

66. Zhou, S., Hamburger, M.: Formation of Sodium Cluster Ions in Electrospray Mass Spectrometry. *Rapid Commun. Mass Spectrom.* **10,** 797-800 (1996)

67. Konermann, L., McAllister, R.G., Metwally, H.: Molecular Dynamics Simulations of the Electrospray Process: Formation of NaCl Clusters via the Charged Residue Mechanism. *J. Phys. Chem. B* **118,** 12025-12033 (2014)

68. Abraham, M.J., Murtola, T., Schulz, R., Páll, S., Smith, J.C., Hess, B., Lindahl, E.: GROMACS: High performance molecular simulations through multi-level parallelism from laptops to supercomputers. *SoftwareX* **1–2,** 19-25 (2015)

69. Huang, J., MacKerell, A.D.: CHARMM36 all-atom additive protein force field: Validation based on comparison to NMR data. *J. Comput. Chem.* **34,** 2135-2145 (2013)

70. Abascal, J.L.F., Vega, C.: A general purpose model for the condensed phases of water: TIP4P/2005. *J. Chem. Phys.* **123,** 234505 (2005)

71. Bauer, B.A., Patel, S.: Molecular dynamics simulations of nonpolarizable inorganic salt solution interfaces: NaCl, NaBr, and NaI in transferable intermolecular potential 4-point with charge dependent polarizability (TIP4P-QDP) water. *J. Chem. Phys.* **132,** 024713 (2010)

72. Jafari-Chermahini, M.T., Tavakol, H.: Adsorption of CO2 on sodium iodide (NaI)(n) (n <= 10) clusters: A density functional theory investigation. *Comput. Theor. Chem.* **1145,** 37-43 (2018)

73. Sattler, K., Muhlbach, J., Echt, O., Pfau, P., Recknagel, E.: Evidence for Coulomb Explosion of Doubly Charged Microclusters. *Phys. Rev. Lett.* **47,** 160-163 (1981)

74. Metwally, H., McAllister, R.G., Popa, V., Konermann, L.: Mechanism of Protein Supercharging by Sulfolane and m-Nitrobenzyl Alcohol: Molecular Dynamics Simulations of the Electrospray Process. *Anal. Chem.* **88,** 5345-5354 (2016)

75. Znamenskiy, V., Marginean, I., Vertes, A.: Solvated Ion Evaporation from Charged Water Droplets. *J. Phys. Chem. A* **107,** 7406-7412 (2003)

76. Patriksson, A., Marklund, E., van der Spoel, D.: Protein Structures under Electrospray Conditions. *Biochemistry* **46,** 933-945 (2007)

77. Steinberg, M.Z., Breuker, K., Elber, R., Gerber, R.B.: The dynamics of water evaporation from partially solvated cytochrome c in the gas phase. *Phys. Chem. Chem. Phys.* **9,** 4690-4697 (2007)

78. Consta, S., Oh, M.I., Kwan, V., Malevanets, A.: Strengths and Weaknesses of Molecular Simulations of Electrosprayed Droplets. *J. Am. Soc. Mass Spectrom.* **29,** 2287-2296 (2018)

79. Kim, D., Wagner, N., Wooding, K., Clemmer, D.E., Russell, D.H.: Ions from Solution to the Gas Phase: A Molecular Dynamics Simulation of the Structural Evolution of Substance P during Desolvation of Charged Nanodroplets Generated by Electrospray Ionization. *J. Am. Chem. Soc.* **139,** 2981-2988 (2017)

80. Porrini, M., Rosu, F., Rabin, C., Darre, L., Gomez, H., Orozco, M., Gabelica, V.: Compaction of Duplex Nucleic Acids upon Native Electrospray Mass Spectrometry. *ACS Central Sci.* **3,** 454–461 (2017)

81. Kondalaji, S.G., Khakinejad, M., Valentine, S.J.: Comprehensive Peptide Ion Structure Studies Using Ion Mobility Techniques: Part 3. Relating Solution-Phase to Gas-Phase Structures. *J. Am. Soc. Mass Spectrom.* **29,** 1665-1677 (2018)

82. Beveridge, R., Migas, L.G., Das, R.K., Pappu, R.V., Kriwacki, R.W., Barran, P.E.: Ion Mobility Mass Spectrometry Uncovers the Impact of the Patterning of Oppositely Charged Residues on the Conformational Distributions of Intrinsically Disordered Proteins. *J. Am. Chem. Soc.* **141,** 4908-4918 (2019)

83. Calixte, E.I., Liyanage, O.T., Kim, H.J., Ziperman, E.D., Pearson, A.J., Gallagher, E.S.: Release of Carbohydrate-Metal Adducts from Electrospray Droplets: Insight into Glycan Ionization by Electrospray. *J. Phys. Chem. B* **124,** 479-486 (2020)

84. Grimm, R.L., Beauchamp, J.L.: Evaporation and Discharge Dynamics of Highly Charged Multicomponent Droplets Generated by Electrospray Ionization. *J. Phys. Chem. A* **114,** 1411-1419 (2010)

85. Jungwirth, P., Tobias, D.J.: Specfic ion effects at the air/water interface. *Chem. Rev.* **106,** 1259-1281 (2006)

86. Kelley, M., Donley, A., Clark, S., Clark, A.: Structure and Dynamics of NaCl Ion Pairing in Solutions of Water and Methanol. *J. Phys. Chem. B* **119,** 15652-15661 (2015)

87. Goth, M., Lermyte, F., Schmitt, X.J., Warnke, S., von Helden, G., Sobott, F., Pagel, K.: Gas-phase microsolvation of ubiquitin: investigation of crown ether complexation sites using ion mobility-mass spectrometry. *Analyst* **141,** 5502-10 (2016)

88. Hamdy, O.M., Julian, R.R.: Reflections on Charge State Distributions, Protein Structure, and the Mystical Mechanism of Electrospray Ionization. *J. Am. Soc. Mass Spectrom.* **23,** 1-6 (2012)

89. Schnier, P.D., Gross, D.S., Williams, E.R.: On the Maximum Charge State and Proton Transfer Reactivity of Peptide and Protein Ions Formed By Electrospray Ionization. *J. Am. Soc. Mass Spectrom.* **6,** 1086-1097 (1995)

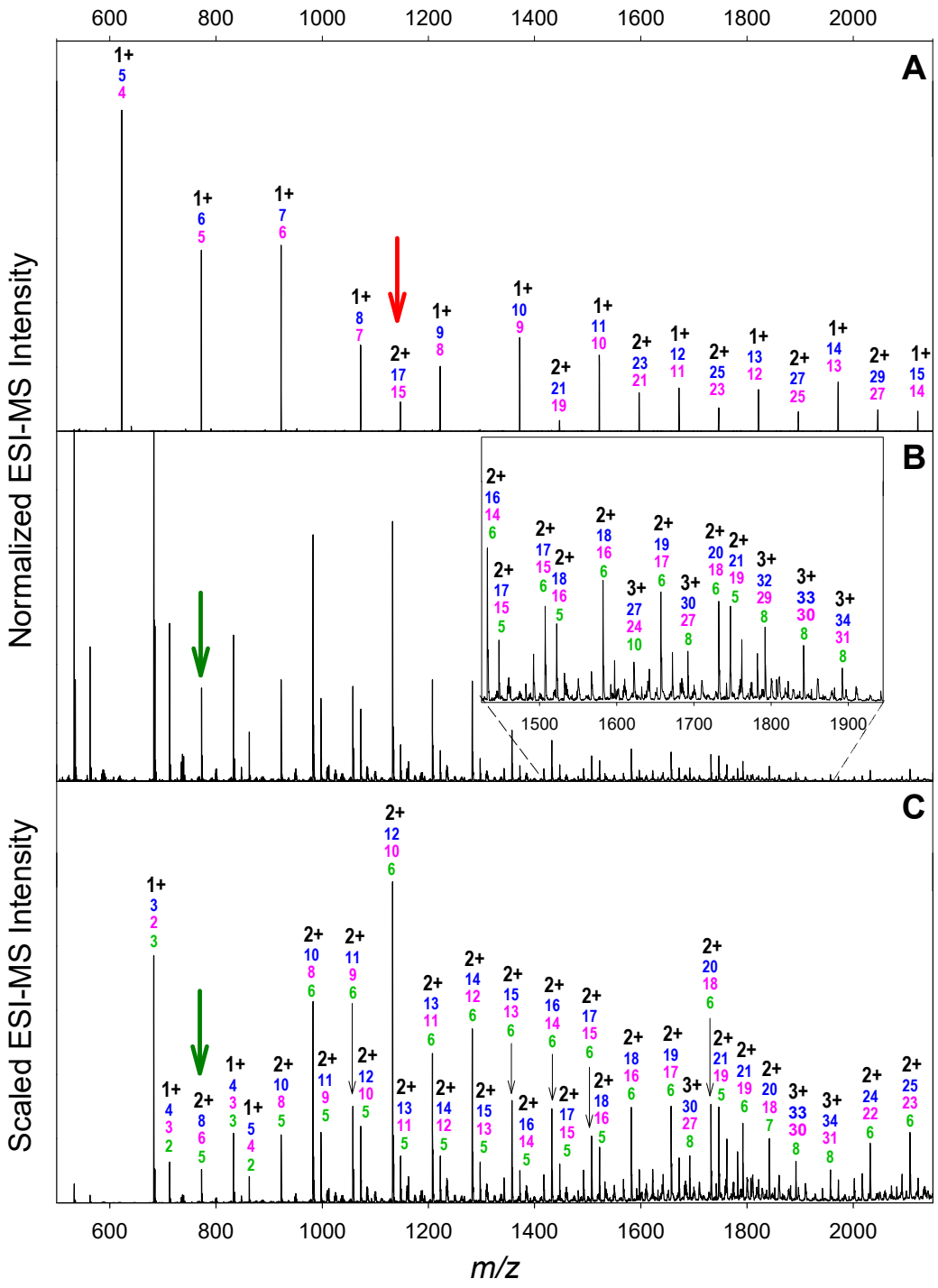

Figure 1. ESI mass spectra of 10 mM NaI acquired under gentle ion sampling conditions (cone voltage = 5 V). (A) water, (B) water with 5% sulfolane. (C) Same as in panel B, but with *y* axis rescaling according to $y = intensity \times (m/z - m/z_{min})$ which boosts the magnitude of low intensity peaks in the high mass range. $[Na_n I_i Sulfolane_s]^{z+}$ clusters are annotated according to their charge *z* (black), number of Na^+ (blue), number of I^- (magenta), and number of sulfolane molecules (green). Arrows indicate the smallest observable 2+ cluster produced from aqueous solution (A) and from water/sulfolane solution (B, C).

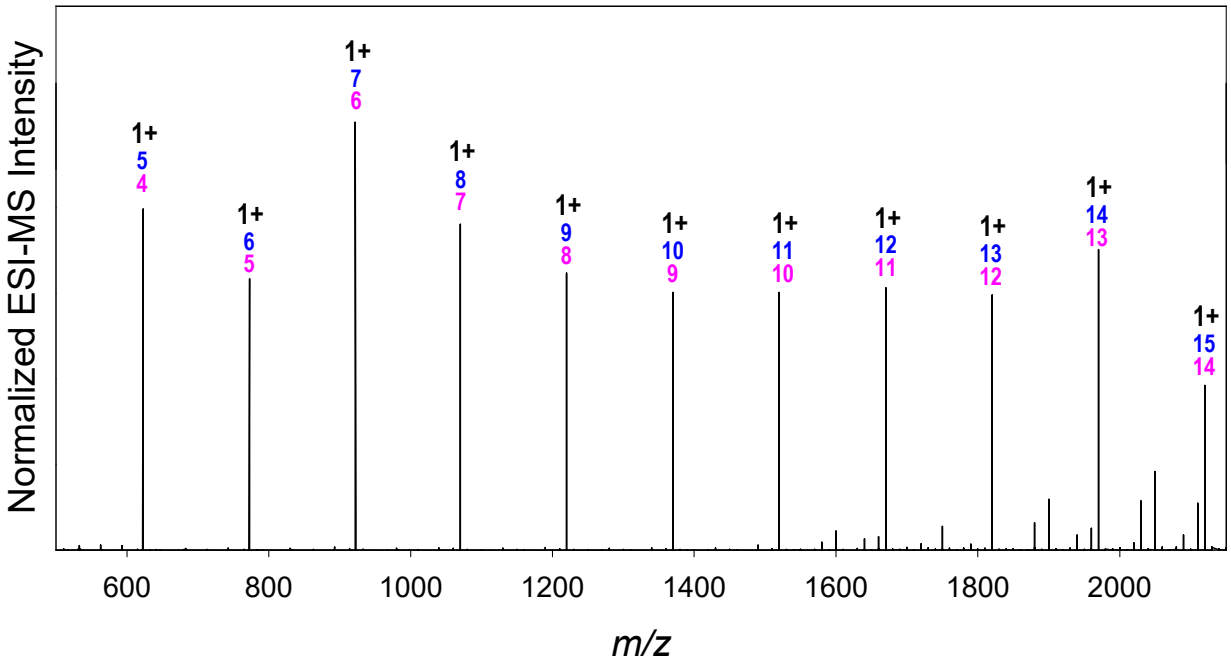

Figure 2. ESI mass spectrum of 10 mM NaI in water with 5% sulfolane acquired using harsh ion sampling conditions (cone voltage = 100 V). Peaks are annotated as in Figure 1.

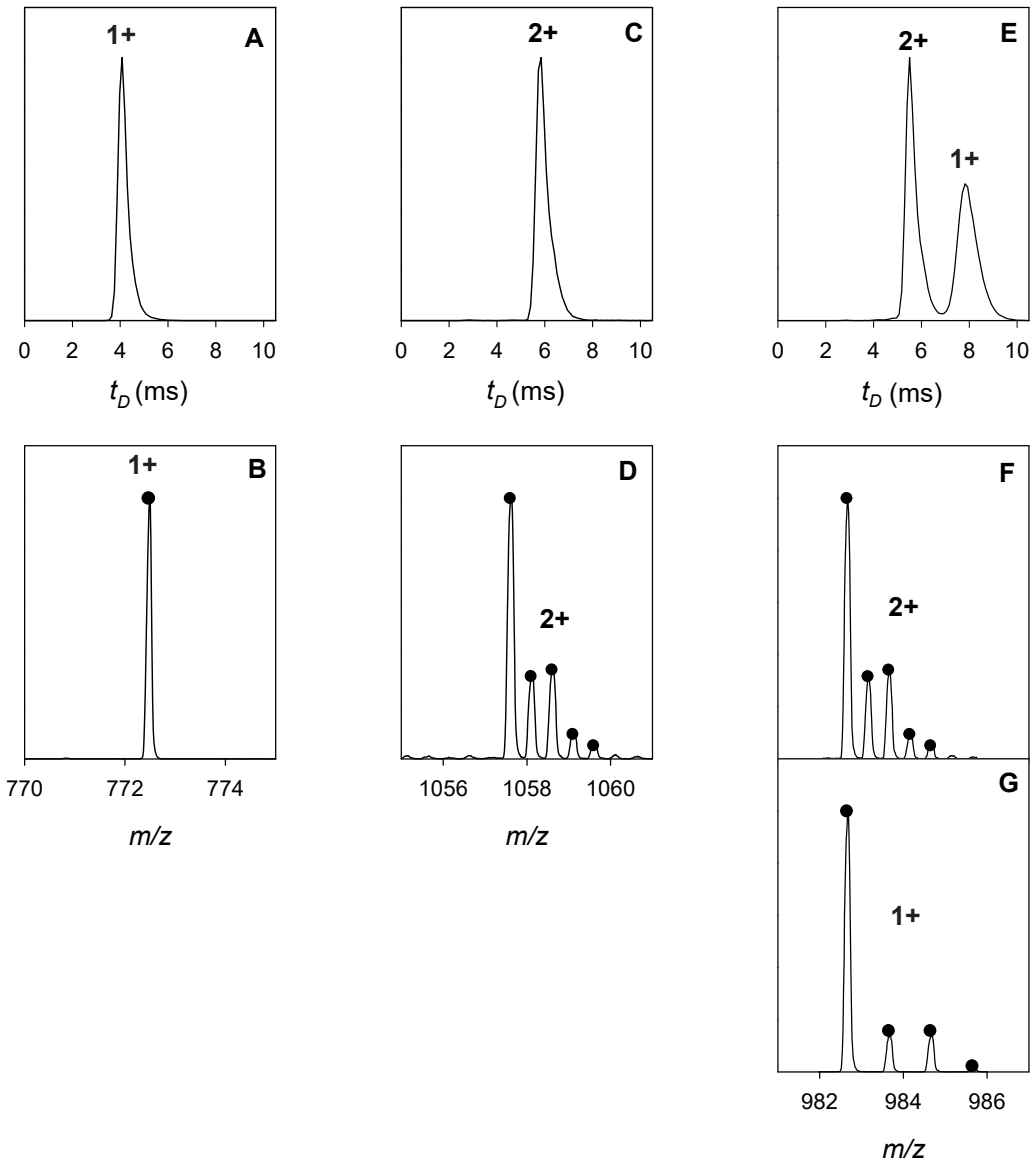

Figure 3. IMS arrival time profiles (drift time t_D vs signal intensity, top row) and MS data (bottom rows) extracted from the IMS profiles for various cluster ions. (A, B) $[Na_5\ I_4]^+$ generated in aqueous solution without sulfolane. (C, D) $[Na_{11}\ I_9\ Sulfolane_6]^{2+}$ generated in the presence of 5% sulfolane. (E-G) Data generated for $[Na_{10}\ I_8\ Sulfolane_6]^{2+}$ and $[Na_5\ I_4\ Sulfolane_3]^+$ which share the same monoisotopic *m/z*. Dots in B/D/F/G represent modeled isotope distributions based on the elemental composition of the various ions.

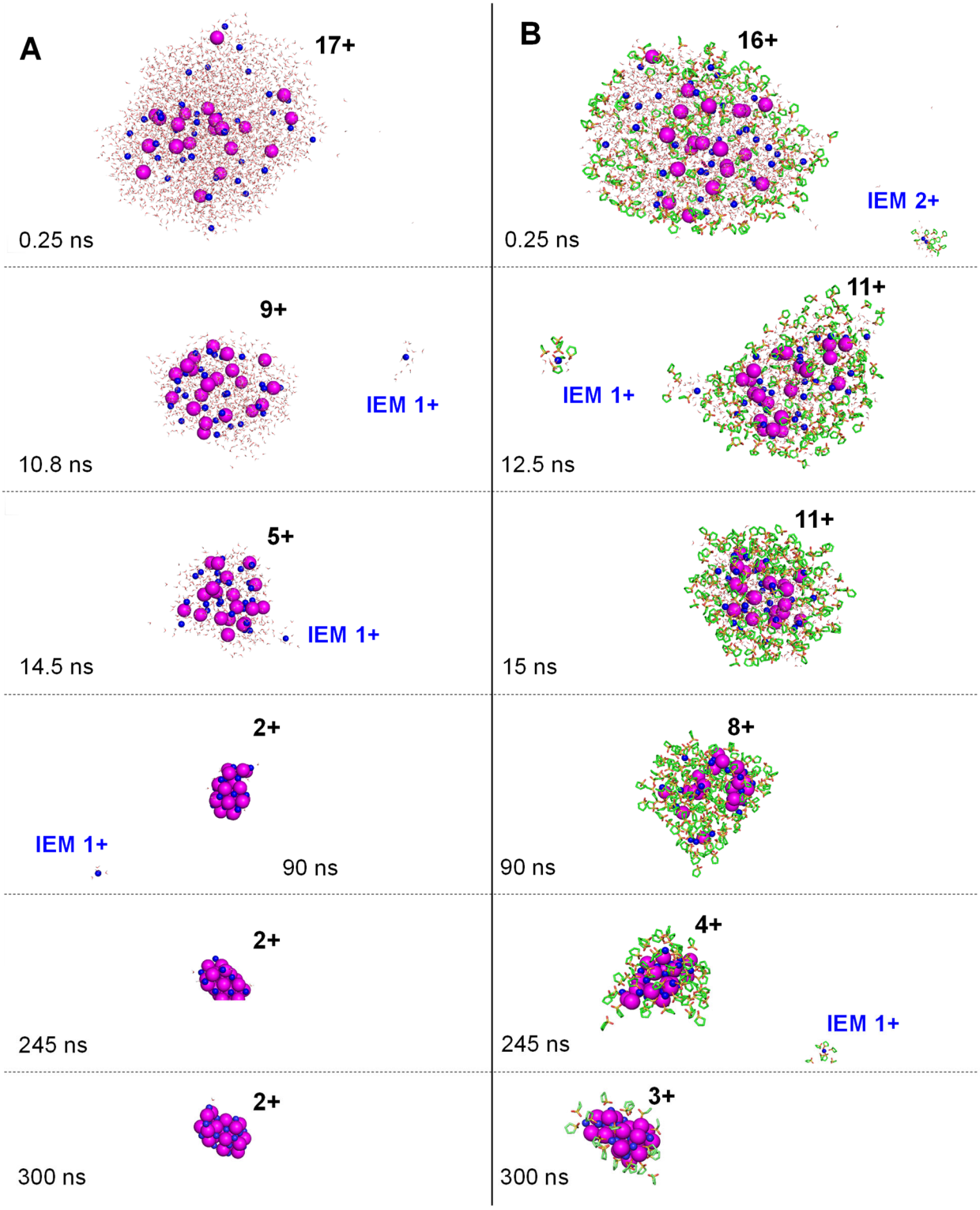

Figure 4. MD simulation snapshots depicting the temporal evolution of ESI droplets with an initial charge of 18+ (38 Na^+ and 20 I^-) in (A) water and (B) water/sulfolane. Field emission events involving solvated Na^+ are marked as "IEM". The droplet or cluster net charge is indicated for each panel. Na^+ (blue) and I^- (magenta) are scaled according to their ionic radii, i.e. 1.02 Å and 2.2 Å, respectively. Sulfolane carbon atoms are shown in green.

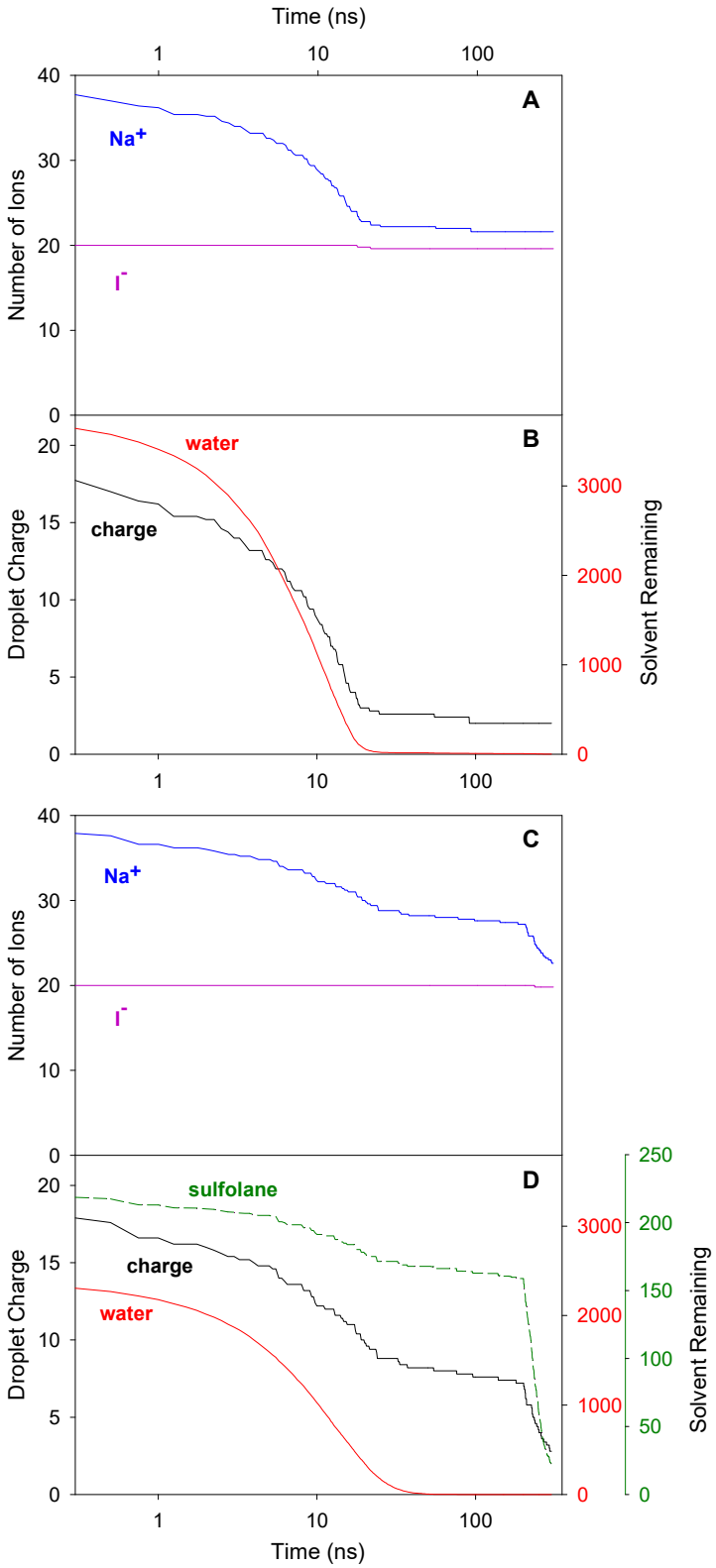

Figure 5. MD data, depicting changes in droplet composition over time, for droplets with an initial ion content of 38 Na^+ and 20 I^-. (A, B) Water droplets. (C, D) Water/sulfolane droplets. Each profile represents an average of five runs. Time axes are scaled logarithmically. Abrupt downward kinks in panels C/D indicate where the temperature was raised from 370 K to 450 K at t = 200 ns.

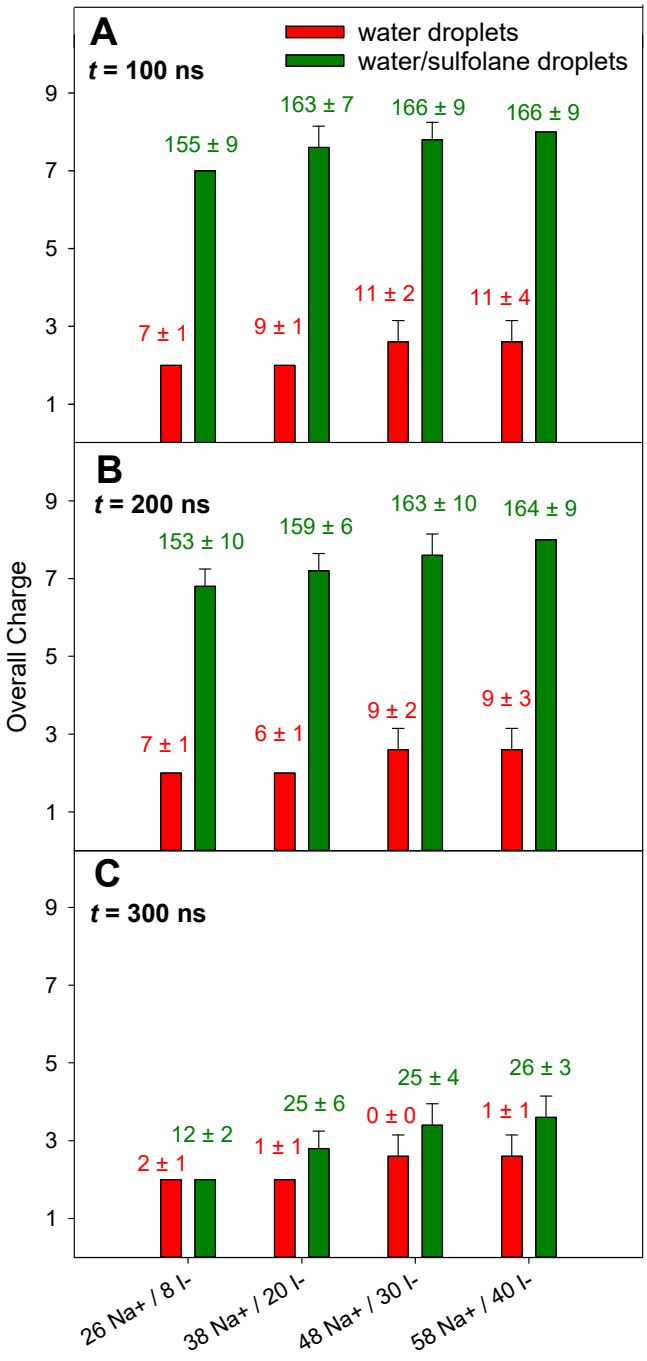

Figure 6. MD data, depicting the droplet (or cluster) charge for various conditions at (A) t =100 ns, (B) t = 200 ns, and (C) t = 300 ns. Results for water droplets are indicated in red, data for water/sulfolane shown in green. The initial number of Na^+ and I^- is shown along the bottom. The number of remaining water or sulfolane molecules is indicated above each bar. Results shown here are averages of five individual runs for each condition. The absence of error bars refers to conditions that consistently yielded the same charge state.

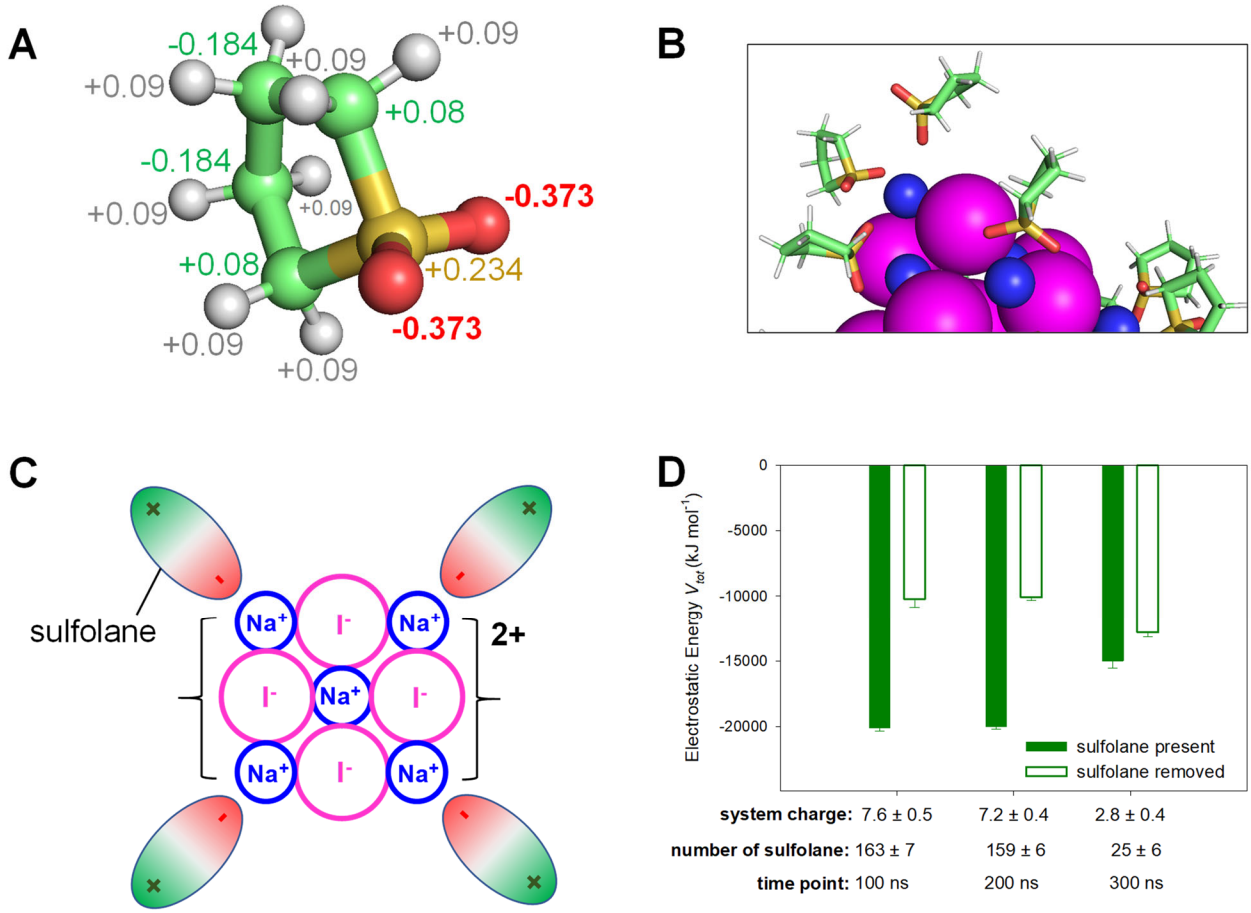

Figure 7. Sulfolane-mediated charge-dipole solvation and stabilization of NaI clusters. (A) Atomic charges in sulfolane (O, red; S, yellow; C, green; H, gray). (B) Close-up of sulfolane interactions with a 3+ cluster, corresponding to t = 300 ns in Fig. 4B. (C) Cartoon representation of sulfolane interactions with a positively charged NaI cluster. (D) Electrostatic energy of NaI clusters at different time points. Solid bars include contributions from all components (Na^+, I^-, and sulfolane); open bars exclude sulfolane contributions.

For Table of Contents Only

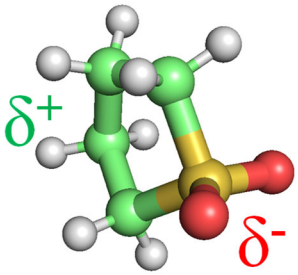

sulfolane dipole

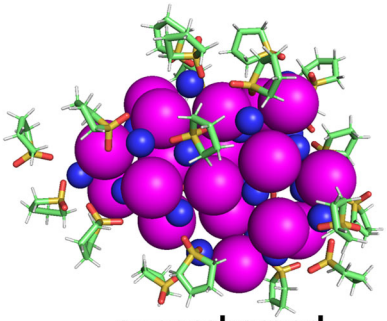

supercharged
NaI cluster